Diamond anvil cell deformation of CaSiO perovskite up to 49 GPa

Lowell Miyagi, Sébastien Merkel, Takehiko Yagi, Nagayoshi Sata, Yasuo Ohishi, Hans-Rudolf Wenk

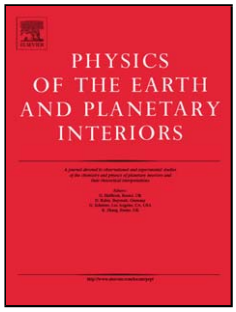

Title: Diamond anvil cell deformation of $CaSiO_3$ perovskite up to 49 GPa

Authors: Lowell Miyagi, Sébastien Merkel, Takehiko Yagi, Nagayoshi Sata, Yasuo Ohishi, Hans-Rudolf Wenk

PII: S0031-9201(08)00116-7
DOI: doi:10.1016/j.pepi.2008.05.018
Reference: PEPI 4959

To appear in: *Physics of the Earth and Planetary Interiors*

Received date: 27-9-2007
Revised date: 7-4-2008
Accepted date: 30-5-2008

Please cite this article as: Miyagi, L., Merkel, S., Yagi, T., Sata, N., Ohishi, Y., Wenk, H.-R., Diamond anvil cell deformation of $CaSiO_3$ perovskite up to 49 GPa, *Physics of the Earth and Planetary Interiors* (2007), doi:10.1016/j.pepi.2008.05.018

Diamond anvil cell deformation of $CaSiO_3$ perovskite up to 49 GPa

Lowell Miyagi [a] Sébastien Merkel [b] Takehiko Yagi [c]
Nagayoshi Sata [d] Yasuo Ohishi [e] Hans-Rudolf Wenk [a]

[a] *Department of Earth and Planetary Science, University of California, Berkeley, CA 94720, United States*

[b] *Laboratoire de Structure et Propriétés de l'Etat Solide, CNRS, Université des Sciences et Technologies de Lille, 59655 Villeneuve d'Ascq, France*

[c] *Institute for Solid State Physics, University of Tokyo, Kashiwanoha 5-1-5, Kashiwa, Chiba 277-8581, Japan*

[d] *Institute for Research on Earth Evolution, Japan Agency for Marine-Earth Science and Technology, Natsushima-cho, Yokosuka, Kanagawa 237-0061, Japan*

[e] *Japan Synchrotron Radiation Research Institute, Mikazuki-cho, Sayo-gun, Hyogo 679-5198, Japan*

Abstract

Radial x-ray diffraction measurements are performed on $CaSiO_3$ perovskite between 25.5 and 49.3 GPa at 300 K. The Rietveld method is used to extract quantitative texture and stress information. We find some mismatches in lattice strains evaluated in the Rietveld method with variations of d-spacings for 200 and 210 over-estimated while those for 111 are under-estimated and attribute it to the effect of plastic deformation. The differential stress supported by $CaSiO_3$ perovskite in this study is approximately twice as large as previous measurements and the ratio of differential stress to shear modulus t/G varies between 5.4% and 7.2% between 25 and 49 GPa. The sample displays preferred orientation of the {100} planes perpendicular to the compression direction, compatible with slip on $\{110\}\langle 1\bar{1}0\rangle$.

Key words: plastic deformation, high pressure, $CaSiO_3$ perovskite, slip, strength, plasticity

1 Introduction

$CaSiO_3$ perovskite is believed to be the major calcium rich phase of the transition zone and lower mantle (Fiquet, 2001; Ricard et al., 2005). Based on laboratory experiments, thermodynamical models, and considerations on the chemical composition of the mantle it is thought to be the third most abundant mineral in the lower mantle, accounting for about 7 wt% of the average composition and up to 20 wt% in subducted slabs (Fiquet, 2001; Ricard et al., 2005; Perrillat et al., 2006). Despite its importance, little is know about this material and its mechanical properties, in large because $CaSiO_3$ is not quenchable to ambient conditions. Previous studies on both the stable structure of $CaSiO_3$ perovskite and its elastic properties have yielded varied results. Early experimental studies reported a cubic unit cell (Liu and Ringwood, 1975; Mao et al., 1989; Tamai and Yagi, 1989). However, first principles calculations predict that lower symmetry, tetragonal or even orthorhombic, structures should be stable (Stixrude et al., 1996; Akber-Knutson et al., 2002; Caracas et al., 2005; Adams and Oganov, 2006; Li et al., 2006b). The calculated structural distortions and energy differences between these structures are small and it is therefore difficult to discern the stable structure (Caracas et al., 2005). Recently, using high resolution synchrotron x-rays, Shim et al. (2002) reported a lower symmetry structure, leading them to propose a tetragonal unit cell. This result was later confirmed by further experimental work (Ono et al., 2004; Kurashina et al., 2004). Accoring to the latest results, the stable structure of $CaSiO_3$ perovskite under ambient temperature is tetragonal with a phase transition to a cubic structure above 490-580 K in the 27 to 72 GPa pressure range (Komabayashi et al., 2007). Studies of the elastic constants of $CaSiO_3$ are limited to theoretical work (Karki and Crain, 1998; Li et al., 2006a) and to date no direct measurements of the elastic constants have been published.

The mechanical properties of high pressure minerals can be studied using radial x-ray diffraction in the diamond anvil cell (DAC) (Merkel et al., 2002). In those experiments, a polycrystalline sample is confined under non-hydrostatic stress in a DAC. The elastic deformation of the crystals is expressed in changes in d-spacings measured on the diffraction images which can be used to estimate the differential stress supported by the sample and provide a lower bound to the yield strength. Plastic deformation by dislocation glide and mechanical twinning produces rotations of crystals and lattice preferred orientation (LPO) which causes intensity variations along the Debye rings. This can be used to infer slip systems and to understand the development of aggregate anisotropy. Radial diffraction studies on the strength of $CaSiO_3$ between 19 and 65 GPa have been performed before (Shieh et al., 2004) but no texture analysis was made. In a previous paper (Miyagi et al., 2006), we presented texture and stress analysis using the Rietveld method with data measured on

a single image at 49.3 GPa. Here we report the full analysis of this experiment with results on the differential stress and development of LPO in $CaSiO_3$ deformed in a DAC from 25.5 to 49.3 GPa.

2 Experiment

Starting material of $CaSiO_3$ wollastonite, ground to a fine powder and mixed with amorphous boron to serve as laser absorber, was loaded into an 80 μm hole in an amorphous boron-epoxy gasket supported by a kapton confining ring (Merkel and Yagi, 2005). Starting thickness of the amorphous boron-epoxy insert was 40 μm with an outer diameter of 400 μm. The sample was compressed with 350 μm diameter culet flat diamonds in a laser heated diamond anvil cell with large openings to allow radial diffraction. The starting material was initially compressed to a pressure of about 20 GPa. At this pressure, the phase transformation to the perovskite phase was induced by single-sided heating with a focused yttrium-aluminum-garnet laser.

Pressure was then increased in 6 steps up to 49.3 GPa at 300 K. Angle-dispersive x-ray diffraction spectra were collected in radial geometry with a 2000x2000 pixels Rigaku R-AXIS IV imaging plate equipped with online reader at beamline BL10XU of SPring-8 using a monochromatic incident x-ray beam (wavelength 0.412 Å) of 20 μm in diameter. The incident x-ray beam was perpendicular to the compression direction and exposure time was about 15 minutes. Sample to detector distance (447.6 mm) and detector tilt were calibrated with a CeO_2 standard taken prior to the experiment. During the reading process in this detector, the imaging plate is rotated within the detector. This results in a shift of the position of the beam center between exposures. In order to accommodate this shift, the direct beam was exposed briefly at the beginning of each exposure and used for beam center calibration.

3 Results

A total of seven diffraction images were taken at 20, 25.5, 29.5, 32.1, 34.8, 43.7, and 49.3 GPa. Of these seven patterns two were unusable due to poor diffraction quality (20 and 34.8 GPa) and were discarded. Representative diffraction spectra are shown in Fig. 1. They show considerable variations in peak position with azimuth angle δ and systematic intensity variations with δ. Variations of peak positions with orientation are related to stress while the variations of diffraction intensity are indicative of LPO in the sample.

Diffraction images were quantitatively analyzed for texture and lattice strains

using the Rietveld method as implemented in the software package MAUD (Lutterotti et al., 1999). Details of the analysis are given in Miyagi et al. (2006) and consequently only relevant features will be discussed here.

Data was fit using a cubic $Pm\bar{3}m$ structure (Finger and Hazen, 1991). Although there may be some minor peak splitting, data quality was too poor to resolve any deviation from the cubic structure, and the data could not be fitted with a tetragonal or orthorhombic structure. The hydrostatic lattice parameter a obtained from the refinement was converted to pressures using a 3rd order Birch-Murnaghan equation of state for $CaSiO_3$ perovskite and values for K_0 and K_0' from Shim et al. (2000).

The variations of peak positions with azimuth were fit using the single crystal elastic constants of Karki and Crain (1998) and the Moment Pole Stress model (Matthies, 1996; Matthies et al., 2001) assuming a 50% Reuss condition. In this analysis, we assumed that the deviatoric component of the stress applied to the sample was

$$\sigma = \begin{bmatrix} \sigma_{11} & 0 & 0 \\ 0 & \sigma_{22} & 0 \\ 0 & 0 & \sigma_{33} \end{bmatrix} \tag{1}$$

with $\sigma_{11} = \sigma_{22}$, and $\sigma_{33} = -2\sigma_{11}$. The differential stress component t was then calculated using

$$t = \sigma_{33} - \sigma_{11}. \tag{2}$$

For comparison with other experiments, we also calculated the angle ψ between the maximum stress direction and the normal to the diffracting plane (e.g. Singh et al., 1998) using

$$\cos\psi = \cos\theta\cos\delta, \tag{3}$$

where θ is the diffraction angle and δ the azimuth on the image plate.

After the first calculation of the stress model, we noticed systematic mismatches in peak positions for the calculated model and the data, such that the azimuthal variation of some peaks were over-estimated while others were under-estimated. For instance, Fig. 2 presents a comparison between the d-spacings obtained using single peak fitting techniques and those recalculated in the Rietveld refinement at 49.3 GPa. The d-spacings for the 200 lines are over-estimated for planes parallel to the compression direction ($\psi \approx 90°$) while

those for 111 are under-estimated at this same orientation. Therefore, we performed new calculations including a refinement of either C_{12} or C_{44}. Both types of refinements equally improved the fit and the results will be presented for the three cases: refinement of t with no refinement of elastic moduli, refinement of t and C_{12}, and refinement of t and C_{44}. In all cases, refinements of t with no elastic moduli provided values between those obtained with C_{12} or C_{44} refined. Therefore, the two stress values obtained C_{12} or C_{44} refined were used to bound the uncertainty in our analysis. We find that the differential stress supported by the sample increases continuously with pressure from a value of 12.1 ($\pm$0.8) GPa at 25.5 GPa to 19.0 ($\pm$1.5) GPa at 49.3 GPa. Table 1 and Fig. 3 summarize these results.

LPO were fit using the E-WIMW algorithm available in MAUD. Initially, no symmetry was imposed and the texture was refined with the other parameters. Textures were found to be approximately axially symmetric about the compression direction (Miyagi et al., 2006). The orientation distribution functions (ODF) were therefore reset and fit with cylindrical symmetry about the compression direction imposed. Textures are moderate with the ODF maxima increasing from 1.38 m.r.d. at 25.5 GPa to 1.61 m.r.d. at 49.3 GPa (Table 1). Texture is conveniently represented by an inverse pole figure of the compression direction which shows the relation between crystallographic directions and the compression direction. The inverse pole figures for all pressures are shown in Fig. 4. In all cases, we find a $<100>$ maximum with a shoulder towards <110> and a depleted region around <111>.

4 Discussion

4.1 Structure

Data was fit using a cubic $Pm\overline{3}m$ structure although first-principles calculations and recent experiments suggest a lower symmetry (Stixrude et al., 1996; Akber-Knutson et al., 2002; Caracas et al., 2005; Adams and Oganov, 2006; Li et al., 2006b; Shim et al., 2002; Ono et al., 2004; Kurashina et al., 2004; Komabayashi et al., 2007). We did investigate the effect of various non-cubic structures on the refinement, $P4/mmm$, $I4/mcm$, $Pnma$, and $Pbnm$. For all cases, it was clear that the cubic structure provided the best match to the data. Consequently, the $Pm\overline{3}m$ structure was retained and used for the refinements. As mentioned before, distortions between the tetragonal and cubic structure are small and it undergoes a phase transition to a cubic structure at higher temperature (Komabayashi et al., 2007). Moreover, the symmetry of the elastic moduli calculated using first-principles methods is consistent with cubic symmetry (Li et al., 2006a). Therefore, it is relevant to use a cubic ref-

erence frame to understand and model the plastic behavior of this phase in the mantle.

4.2 Stress

We find some mismatches in peak positions between the calculated model and the data, such that the azimuthal variation of some peaks are over-estimated while others were under-estimated (Fig. 2). Better results are obtained by including a fit of the shear related constants C_{12} and C_{44}, with both refinements equally improving the fit. Still, it can be seen that the amplitude of the variations of d-spacings is not fully accounted for (e.g. 111, 200, 210).

There are sereval reasons to account for these mismatches. First, we assumed a cubic symmetry and this could have an effect on the stress model. Second, errors in the calculations of elastic moduli we used (Karki and Crain, 1998) could also affect the stress model. However, the variations we observe in the refinement on the elastic moduli (up to 20% for C_{12} and up to 12% for C_{44}) are larger than what is usually expected for first-principles calculations on silicates. Third, it has been shown that errors in the calculation of stress models can occur if there is a small component of shear within the sample or if the axis of maximum compression deviates from the diamond axis (Merkel, 2006). It is most likely that those mismatches are due to yield strength anisotropy. It has been shown that stresses deduced using x-ray diffraction on materials that deform plastically can be drastically different when using different lattice planes (Weidner et al., 2004; Li et al., 2004; Merkel et al., 2006). In particular, Weidner et al. (2004) and Li et al. (2004) demonstrated that, for MgO, stresses deduced from 200 would be significantly smaller than those deduced from 111. This is in agreement with our measurements on $CaSiO_3$ perovskite where we over-estimate the amplitude of the variations of d-sacings for 200 and 210 while those for 111 are under-estimated.

Plastic deformation induces errors in x-ray stress measurements that can be difficult to account for. In this study, we decided to use the average stress obtained from the refinements using fixed elastic moduli, with C_{12} refined, and with C_{44} refined. The difference between the values we obtained are on the order of 10% and were used to estimate an error on our measurements (Table 1). In any case, mismatches in the stress model may also induce errors in texture calculation and thus is important to remedy prior to extraction of texture information (Miyagi et al., 2006). It should be noted that the values of C_{12} and C_{44} refined with the x-ray data are empirical and represent effective elastic moduli that can fit our data. They are not directly related to single crystal elastic moduli (Li et al., 2004; Merkel et al., 2006; Antonangeli et al., 2006).

4.3 Strength

By the von Mises yield criterion the measured differential stress supported by a sample provides a lower bounds estimate for the yield strength. For the case of axial compression this is $t = \sigma_3 - \sigma_1 \leq \sigma_y$ where σ_y is the yield strength. If plastic deformation is achieved then the yield strength is equal to the maximum differential stress. Yield strength in a polycrystal depends on the available slip systems, their critical resolved shear stress (CRSS), and as well as the texture of the sample. Hardening or an increase in the yield strength can also result if the dislocation density of the sample increases (Kocks and Mecking, 2003). It is important to note that strain, strain rate, and pressure cannot be decoupled in our experiment and we must use a general definition of yield strength.

The values of differential stress supported by our sample are about twice as large as those of Shieh et al. (2004) (Fig. 3) and this observation is independent of the assumption used to deduce stress from the x-ray data, as our data shows significantly more variations of d-spacings with orientation (Fig. 2). In DAC experiments, the plastic yield limit is not always reached between the tips of the diamonds (Merkel et al., 2000). Therefore, lower values of differential stress may be obtained. Hardening due to an increase in dislocation density may also result in a higher yield strength and may affect the value of t. In our experiment, the sample was mixed with boron, while Shieh et al. (2004) added platinum to the sample. Platinum may have acted as a softer phase and accommodated some of the strain. It may also coat grains and promote deformation mechanisms such as grain boundary sliding that would prevent $CaSiO_3$ from reaching its yield point. Choice of gasket material may also affect the value of t, as a harder gasket material may support more stress, preventing the sample from reaching the yield point.

In order to compare the strengths of a range of materials the dimensionless quantity t/G is often used, where t is the differential stress and G is the shear modulus (e.g. Ruoff, 1973; Chua and Ruoff, 1975). In general this ratio tends to be in the 3-7% range for silicates and less than 3% for metals. Our value for $CaSiO_3$ perovskite is 5.4% at 25.5 GPa and becomes as high as 7.2% at 49.3 GPa, in the range of values obtained for other silicates and oxides (Fig. 5).

4.4 Texture

Texture strength increases with pressure and shows no indication of saturation with increasing stress. No change in texture type with pressure increase is observed. In order to interpret our experimental textures we use the viscoplas-

tic self-consistent polycrystal plasticity model (Lebensohn and Tomé, 1993) to simulate texture evolution in cubic perovskite polycrystal deformed by slip under axial compression. The experimental texture pattern of $CaSiO_3$ perovskite in axial compression is similar to textures obtained for MgO (Merkel et al., 2002), a cubic minerals with low temperature slip systems of $\{110\}<1\bar{1}0>$. This is the same slip system that has been proposed for cubic perovskites at low temperature (Poirier et al., 1989) and observed at high temperature in $CaTiO_3$ (Besson et al., 1996) and $SrTiO_3$ (Wang et al., 1993). Consequently we chose to investigate deformation on these slip systems, as well as other slip systems common in cubic minerals. These include $\{111\}<1\bar{1}0>$ (the dominant slip system in minerals with fcc structure), $\{110\}<1\bar{1}1>$ (common in bcc structures), $\{110\}<1\bar{1}0>$ (MgO), $\{100\}<011>$ (galena), and $\{100\}<001>$ (pyrite). We find that only simulations that favor slip on $\{110\}<1\bar{1}0>$ produce textures that are very similar to the experimental results. We conclude that $\{110\}<1\bar{1}0>$ is most likely the dominant slip plane in pseudo-cubic $CaSiO_3$ perovskite.

This is in agreement with previous observations that the texture pattern for $CaSiO_3$ is compatible with dominant slip on $\{110\}<1\bar{1}0>$ (Miyagi et al., 2006, Fig. 5). It is interesting to note that, for this system, each slip plane and direction has an equivalent and opposite slip plane and direction e.g. $(110)[1\bar{1}0]$ and $(1\bar{1}0)[110]$. These equivalent systems have the same Schmid factor and their spins cancel each other. As a result texture does not develop due to shears on this slip system. Slip on this system does however induce an orientation dependent change in grain shape which leads to shape dependent reorientation. As texture develops due to grain shape changes, textures are weak at low strains but, at higher strains, grains become more elongated and stronger textures can develop (Wenk, 2000). Indeed, this is consistent with the moderate texture strengths observed here (up to 1.7 m.r.d.) since our deformation geometry only allows an approximate 20% strain (Wenk et al., 2006).

5 Conclusions

We performed radial x-ray diffraction on $CaSiO_3$ perovskite under non-hydrostatic loading between 25.5 and 49.3 GPa and analysed the data using the Rietveld method, as implemented in the software MAUD (Lutterotti et al., 1999). We investigated the effect of various non-cubic structures on the refinement and found that, for all cases, the cubic structure $Pm\bar{3}m$ provided the best match to the data. It should be noted, however, that our sample was highly stressed and that the data quality could have been too poor to resolve the small distortions between the proposed cubic and tetragonal structures (Shim et al., 2002; Komabayashi et al., 2007).

We find some mismatches between lattice strains evaluated in MAUD and the experimental data, with variations of d-spacings for 200 and 210 over-estimated while those for 111 are under-estimated. Better results are obtained by including a fit of the shear related constants C_{12} or C_{44}. This is attributed to the effect of plastic deformation on lattice strains, as previously noticed in MgO (Weidner et al., 2004; Li et al., 2004) and cobalt (Merkel et al., 2006).

The differential stress supported by $CaSiO_3$ perovskite in this study is approximately twice as large as previous measurements (Shieh et al., 2004). The ratio of differential stress to shear modulus t/G varies between 5.4% and 7.2% between 25 and 49 GPa. This highlights the importance of insuring that samples reach the plastic yield point when deducing the yield strength of a material. It also indicates that the addition of a second phase, amorphous boron in this work and platinum in that of Shieh et al. (2004), may have a significant effect on measurements of strength.

Our results indicate that, at high pressure and room temperature, significant texture can be induced in $CaSiO_3$ perovskite. We obtained texture patterns with a $<100>$ maximum, a shoulder towards $<110>$, and a depleted region around $<111>$. Comparison with visco-plastic self-consistent modeling indicates that this texture is most likely due to dominant slip on $\{110\}<1\bar{1}0>$.

6 Acknowledgements

The authors wish to thank N. Funamori for providing the starting material. The synchrotron radiation experiments were performed at the BL10XU in SPring-8 with the approval of the Japan Synchrotron Radiation Research Institute (JASRI) (Proposal No. 2003B0243-ND2b-np). L. M. acknowledges support from the Carnegie DOE Alliance Center (CDAC). S. M. acknowledges support from the Japanese Society for the Promotion of Science and The Miller Institute for Basic Research in Science at UC Berkeley.

References

Adams, D. J., Oganov, A. R., 2006. Ab initio molecular dynamics study of $CaSiO_3$ perovskite at P-T conditions of earth's lower mantle. Phys. Rev. B 73, 184106.

Akber-Knutson, S., Bukowinski, M. S. T., Matas, J., 2002. On the structure and compressibility of $CaSiO_3$ perovskite. Geophys. Res. Lett. 29, 1034.

Antonangeli, D., Merkel, S., Farber, D. L., 2006. Elastic anisotropy in hcp metals at high pressure and the sound wave anisotropy of the earth's inner core. Geophys. Res. Lett. 33, L24303.

Besson, P., Poirier, J. P., Price, G. D., 1996. Dislocations in $CaTiO_3$ perovskite deformed at high temperature: a transmission electron microscopy study. Phys. Chem. Min. 23, 337–344.

Caracas, R., Wentzcovitch, R., Price, G. D., Brodholt, J., 2005. $CaSiO_3$ perovskite at lower mantle pressures. Geophys. Res. Lett. 32, L06306.

Chua, J. O., Ruoff, A. L., 1975. Pressure dependence of the yield stress of potassium at low homologous temperature. J. Appl. Phys. 46, 4659–4663.

Finger, L. W., Hazen, R. M., 1991. Crystal chemistry of six-coordinated silicon: a key to understanding the earth's deep interior. Acta Cryst. B47, 561–580.

Fiquet, G., 2001. Mineral phases of the Earth's mantle. Z. Kristallogr. 216, 248–271.

Karki, B. B., Crain, J., 1998. First-principles determination of elastic properties of $CaSiO_3$ perovskite at lower mantle pressures. Geophys. Res. Lett. 25, 2741274.

Kavner, A., Duffy, T. S., 2001. Strength and elasticity of ringwoodite at upper mantle pressures. Geophys. Res. Lett. 28, 2691–2694.

Kocks, U. F., Mecking, H., 2003. Physics and phenomenology of strain hardening: the fcc case. Prog. Mater Sci. 48, 171–273.

Komabayashi, T., Hirose, K., Sata, N., Ohishi, Y., Dubrovinsky, L. S., 2007. Phase transition in $CaSiO_3$ perovskite. Earth Planet. Sci. Lett. 260, 564–569.

Kurashina, T., Hirose, K., Ono, S., Sata, N., Ohishi, Y., 2004. Phase transition in al-bearing $CaSiO_3$ perovskite: implications for seismic discontinuities in the lower mantle. Phys. Earth Panet. Inter. 145, 67–74.

Lebensohn, R. A., Tomé, C. N., 1993. A selfconsistent anisotropic approach for the simulation of plastic deformation and texture development of polycrystals: application to zirconium alloys. Acta Metall. Mater. 41, 2611–2624.

Li, L., Weidner, D. J., Brodholt, J., Alfé, D., Price, G. D., Caracas, R., Wentzcovitch, R., 2006a. Elasticity of $CaSiO_3$ perovskite at high pressure and high temperature. Phys. Earth Panet. Inter. 155, 249–259.

Li, L., Weidner, D. J., Brodholt, J., Alfè, D., Price, G. D., Caracas, R., Wentzcovitch, R., 2006b. Phase stability of $CaSiO_3$ perovskite at high pressure and temperature: Insights from ab initio molecular dynamics. Phys. Earth Panet. Inter. 155, 260–268.

Li, L., Weidner, D. J., Chen, J., Vaughan, M. T., Davis, M., Durham, W. B.,

2004. X-ray strain analysis at high pressure: Effect of plastic deformation in mgo. J. Appl. Phys. 95, 8357–8365.

Liu, L.-G., Ringwood, A. E., 1975. Synthesis of a perovskite-type polymorph of $CaSiO_3$. Earth Planet. Sci. Lett. 28, 209–211.

Lutterotti, L., Matthies, S., Wenk, H. R., 1999. Maud: a friendly java program for materials analysis using diffraction. Int. U. Crystallogr. Comm. Powder Diffr. Newslett. 21, 14 – 15.

Mao, H. K., Shen, L. C., Hemley, R. J., Jephcoat, A. P., Wu, Y., 1989. Stability and equation of state of $CaSiO_3$ perovskite to 134 GPa. J. Geophys. Res. 94, 17889–17894.

Matthies, S., 1996. Moment pole figures in residual stress analysis. Textures and Microstructures 25, 229–236.

Matthies, S., Priesmeyer, H. G., Daymond, M. R., 2001. On the diffractive determination of single-crystal elastic constants using polycrystalline samples. J. Appl. Cryst. 34, 585–601.

Merkel, S., 2006. X-ray diffraction evaluation of stress in high pressure deformation experiments. J. Phys.: Condens. Matter 18, S949–S962.

Merkel, S., Hemley, R. J., Mao, H. K., Teter, D. M., 2000. Finite element modeling and ab-initio calculations of megabar stresses in the diamond anvil cell. In: Manghnani, M., Nellis, W. J., Nicol, M. F. (Eds.), Science and Technology of High Pressure Research. University Press (India) Limited, pp. 68–73.

Merkel, S., Miyajima, N., Antonangeli, D., Fiquet, G., Yagi, T., 2006. Lattice preferred orientation and stress in polycrystalline hcp-Co plastically deformed under high pressure. J. Appl. Phys. 100, 023510.

Merkel, S., Wenk, H. R., Badro, J., Montagnac, G., Gillet, P., Mao, H. K., Hemley, R. J., 2003. Deformation of $(Mg,Fe)SiO_3$ perovskite aggregates up to 32 GPa. Earth Planet. Sci. Lett. 209, 351–360.

Merkel, S., Wenk, H. R., Shu, J., Shen, G., Gillet, P., Mao, H. K., Hemley, R. J., 2002. Deformation of polycrystalline MgO at pressures of the lower mantle. J. Geophys. Res. 107, 2271.

Merkel, S., Yagi, T., 2005. X-ray transparent gasket for diamond anvil cell high pressure experiments. Rev. Sci. Instrum. 76, 046109.

Miyagi, L., Merkel, S., Yagi, T., Sata, N., Ohishi, Y., Wenk, H. R., 2006. Quantitative Rietveld texture analysis of $CaSiO_3$ perovskite deformed in a diamond anvil cell. J. Phys.: Condens. Matter 18, S995–S1005.

Ono, S., Ohishi, Y., Mibe, K., 2004. Phase transition of ca-perovskite and stability of al-bearing mg-perovskite in the lower mantle. Am. Mineral. 89, 14801485.

Perrillat, J.-P., Ricolleau, A., Daniel, I., Fiquet, G., Mezouar, M., Guignot, N., Cardon, H., 2006. Phase transformations of subducted basaltic crust in the upmost lower mantle. Phys. Earth Panet. Inter. 157, 139–149.

Poirier, J. P., Beauchesne, S., Guyot, F., 1989. Deformation mechanisms of crystals with perovskite structure. In: Navrotsky, A., Weidner, D. (Eds.), Perovskite: a structure of great interest to geophysics and materials science.

AGU, Washington DC, pp. 119–123.

Ricard, Y., Mattern, E., Matas, J., 2005. Synthetic tomographic images of slabs from mineral physics. In: van der Hilst, R. D., J.Bass, Matas, J., Trampert, J. (Eds.), Earth's Deep Mantle: Structure, Composition, and Evolution. Vol. 160 of AGU Geophys. Monograph Series. AGU, pp. 283–300.

Ruoff, A. L., 1973. Penultimate static pressure containment considerations and possible application to metallic hydrogen preparation. Adv. Cryog. Eng. 18, 435–440.

Shieh, S., Duffy, T. S., Li, B., 2002. Strength and elasticity of SiO_2 across the stishovite-$CaCl_2$-type structural phase boundary. Phys. Rev. Lett. 89, 255507.

Shieh, S. R., Duffy, T. S., Shen, G., 2004. Elasticity and strength of calcium silicate perovskite at lower mantle pressures. Phys. Earth Panet. Inter. 143-144, 93–105.

Shim, S. H., Duffy, T. S., Shen, G., 2000. The stability and P-V-T equation of state of $CaSiO_3$ perovskite in the Earth's lower mantle. J. Geophys. Res. 105, 25955–25968.

Shim, S. H., Jeanloz, R., Duffy, T. S., 2002. Tetragonal structure of $CaSiO_3$ perovskite above 20 GPa. J. Geophys. Res. 29, doi:10.1029/2002GL016148.

Singh, A. K., Balasingh, C., Mao, H. K., Hemley, R. J., Shu, J., 1998. Analysis of lattice strains measured under non-hydrostatic pressure. J. Appl. Phys. 83, 7567–7575.

Stixrude, L., Cohen, R. E., Yu, R., Krakauer, H., 1996. Prediction of phase transition in $CaSiO_3$ perovskite and implications for lower mantle structure. Am. Mineral. 81, 1293–1296.

Tamai, H., Yagi, T., 1989. High-pressure and high-temperature phase relations in $CaSiO_3$ and $CaMgS_2O_6$ and elasticity of perovskite-type $CaSiO_3$. Phys. Earth Panet. Inter. 54, 370–377.

Uchida, T., Funamori, N., Ohtani, T., Yagi, T., 1996. Differential stress of MgO and Mg_2SiO_4 under uniaxial stress field: Variation with pressure, temperature, and phase transition. In: Trzeciatowski, W. A. (Ed.), High Pressure Science and Technology. World Scientific Publishing, Singapore, pp. 183–185.

Wang, Z., Karato, S., Fujino, F., 1993. High temperature creep of single crystal strontium titanate ($SrTiO_3$): a contribution to creep systematics in perovskites. Phys. Earth Panet. Inter. 79, 299–312.

Weidner, D. J., Li, L., Davis, M., Chen, J., 2004. Effect of plasticity on elastic modulus measurements. Geophys. Res. Lett. 31, L06621.

Wenk, H. R., 2000. Plasticity modeling in minerals and rocks. In: Kocks, U. F., Tomé, C. N., Wenk, H. R. (Eds.), Texture and Anisotropy: Preferred Orientaions in Polycrystals and Their Effect on Materials Properties, 2nd Edition. Cambridge University Press, Cambridge, Ch. 14, pp. 560–596.

Wenk, H. R., Lonardelli, I., Merkel, S., Miyagi, L., Pehl, J., Speziale, S., Tommaseo, C. E., 2006. Deformation textures produced in diamond anvil exper-

iments, analysed in radial diffraction geometry. J. Phys.: Condens. Matter 18, S933–S947.

P	C_{11}	C_{12}	C_{44}	Min	Max	t	C_{12} refined		C_{44} refined		$<t>$
							t	C_{12}	t	C_{44}	
25.5	554	234	274	0.77	1.38	12.3	11.3	275	12.9	314	12.1 ± 0.8
29.5	583	245	280	0.70	1.43	12.9	10.7	325	14.2	362	12.4 ± 1.7
32.1	601	251	285	0.77	1.53	14.7	14.8	249	14.7	283	14.7 ± 0.1
43.7	681	280	303	0.78	1.65	17.7	18.9	230	16.8	272	16.8 ± 1.0
49.3	712	292	311	0.71	1.61	18.8	20.6	221	17.5	264	17.5 ± 1.5

Table 1
Pressure, corresponding elastic moduli C_{11}, C_{12}, and C_{44} (Karki and Crain, 1998), ODF minima and maxima, and differential stresses t fitted to the data. Table also includes results for differential stresses and elastic moduli for refinements including C_{12} or C_{44}. $<t>$ is the final estimate of differential stress based on the results obtained for various hypothesis. Pressures, elastic moduli, and stresses are expressed in GPa, ODF minima and maxima in m.r.d. Note that the refined elastic moduli C_{12} or C_{44} are effective moduli which reproduce the x-ray data and do not directly correspond to single crystal elastic moduli.

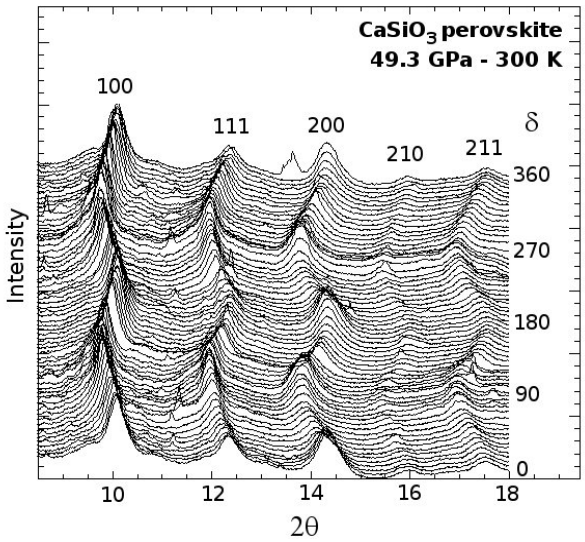

Fig. 1. Diffraction spectra extracted from the diffraction pattern at 49.3 GPa for azimuth angles δ between 0° and 360° with 5° intervals. Diffraction lines from the $CaSiO_3$ perovskite sample are indicated on the figures. Variations of diffraction intensities and peak positions with orientation are related to LPO and stress in the sample, respectively. Unlabelled peak at $2\theta \approx 13.5°$ and $\delta = 360°$ is a diamond spot.

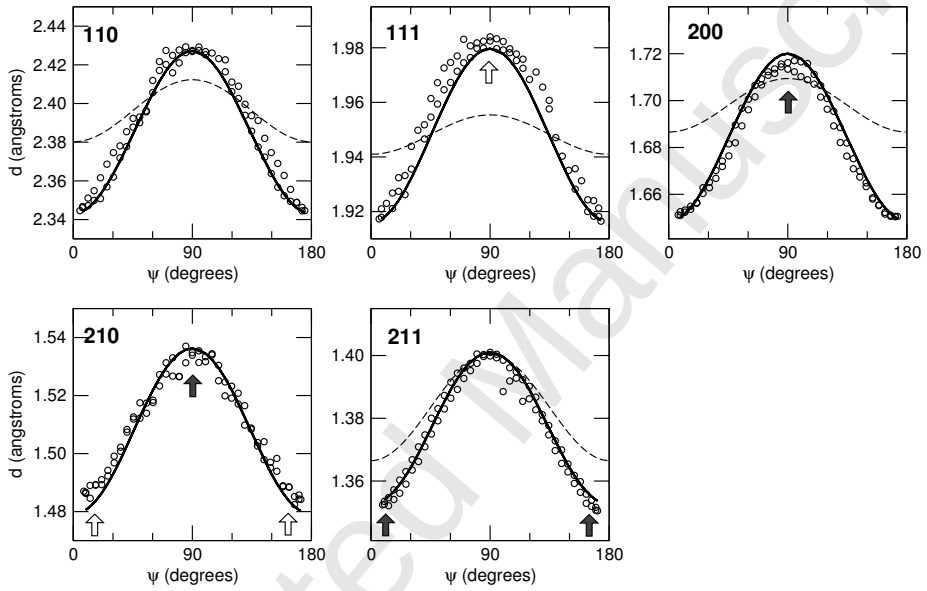

Fig. 2. D-spacings vs. angle between the diffracting plane normal and the maximum stress axis ψ at 49.3 GPa. Open circles were extracted from the diffraction spectra using single peak fitting. Thick solid lines is recalculated from the Rietveld refinement with C_{12} or C_{44} refined. Thin dashed lines are fit to the results at 52 GPa from Shieh et al. (2004). Differences between refinements with with no C_{ij} refined, C_{12} refined, or C_{44} refined can not be seen at this scale. White and dark arrows indicate orientations where the peak positions are under- and over-estimated, respectively.

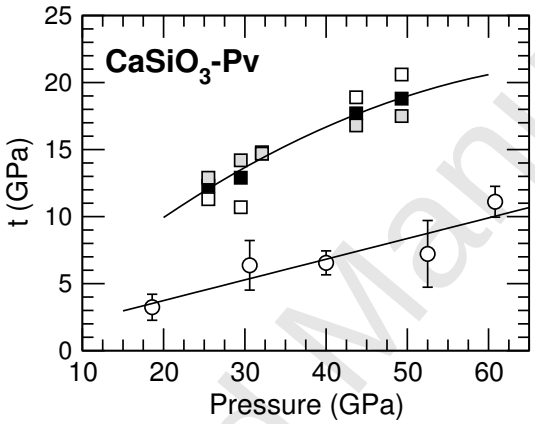

Fig. 3. Differential stress measured in $CaSiO_3$ perovskite. Squares are data from this study calculated using the elastic moduli of Karki and Crain (1998), with no refinement of elastic moduli (black squares), refining C_{12} (white squares), and refining C_{44} (grey squares). Circles are the results from Shieh et al. (2004). Solid lines are guide to eyes through the data.

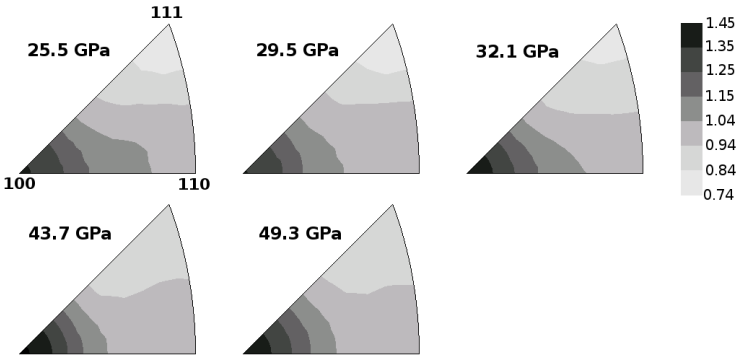

Fig. 4. Inverse pole figure of the compression direction illustrating the LPO in cubic $CaSiO_3$ perovskite compressed in a diamond anvil cell for all pressures measured in this study. Equal area is used and linear contours are expressed in multiples of random distribution.

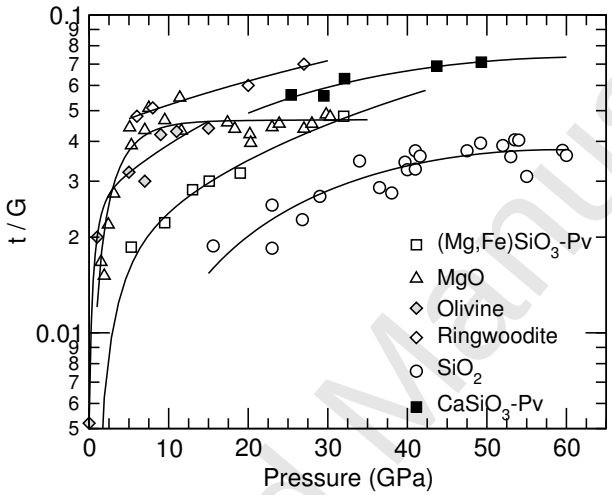

Fig. 5. Ratio of differential stress to shear modulus t/G as a function of pressure obtained in radial diffraction experiments in the DAC. Solid squares are measurements on $CaSiO_3$ perovskite from this study, open squares results for (Mg,Fe)SiO_3 perovskite (Merkel et al., 2003), open triangles results for MgO (Merkel et al., 2002), grey diamonds results for olivine (Uchida et al., 1996), open diamonds results for ringwoodite (Kavner and Duffy, 2001), and open circles results for SiO_2 (Shieh et al., 2002). Lines are guides to the eyes through the experimental data.